CRYO/99/012
February 20, 1999

Numerical Quenchback in Thermofluid Simulations of Superconducting Magnets

L. Bottura, A. Shajii

Distribution: Internal

Published: Int. J. Num. Meth. Eng.ng, **43**, 1275-1293, 1998

Summary

One of the most important thermofluid processes encountered in internally cooled superconducting magnets is that of quenching. Numerical simulation of the quench propagation involves accurately modeling a moving boundary layer at the quench front. Due to the highly non-linear nature of the quench process, slightest numerical errors can rapidly grow to unacceptable limits. The quench propagation in such a non-converged solution exhibits a very rapid propagation velocity which resembles a "quenchback" effect. Hence, the term "Numerical Quenchback" is used to characterize a numerically unstable solution of the governing quench model. This paper presents the underlying physical phenomena that causes a numerical discretization scheme to have error terms that increase exponentially with time, causing the numerical quenchback effect. Specifically, by analytically solving the equivalent differential equation of the numerical scheme, we are able to obtain closed form relations for the error terms associated with the propagation velocity. This allows us to define error criteria on the space and time steps used in the simulation. The reliability of the error criteria is proven by detailed convergence studies of the quench process.

1. Introduction

Superconducting magnets cooled by a force-flow of helium can occasionally and locally make a transition to the normal resistive state, where they begin to generate Joule heating at exceedingly high rates. The initial *normal conducting* zone propagates in the magnet because of expulsion of the heated helium and, in part, thermal conduction at the normal-front. The detection of an electrical resistance due to the normal zone in the magnet usually triggers protection systems which disconnect the power supply and discharge the magnetic energy through an external resistor. This describes schematically the process of *quench* in superconducting magnets [1].

The simplest model of the initiation and evolution of a quench in a force-flow cooled superconducting cable is based on a 1-D schematization of the superconductor along its length (see Refs. [2-5] for details). The superconducting cable temperature is obtained in general from a non-stationary, non-linear heat conduction equation. The source terms in this equation are the Joule heat in the cable and the heat transfer to the helium. The helium flow is described by mass, momentum and energy balances in the form of the Euler equations, with the addition of source terms modelling the frictional

pressure drop along the cable and heat exchange with the superconducting cable. The flow in force-flow cooled is usually highly turbulent, with high heat transfer between cable and helium. Hence, for simplicity, we assume here that the helium and the cable have the same temperature and we neglect the influence of the structural cable components (i.e. conduit wall). Finally, we neglect inertial effects in the coolant, and we arrive to the following set of equations describing the thermal and hydraulic processes during a quench [4]:

$$\frac{\partial \rho}{\partial t} + \frac{\partial \rho v}{\partial x} = 0 \tag{1}$$

$$\frac{\partial p}{\partial x} = -\frac{2f}{D_h}\rho v|v| \tag{2}$$

$$\rho \hat{C}_t \frac{\partial T}{\partial t} + \rho \hat{C}_v v \frac{\partial T}{\partial x} + \rho \hat{C}_v \phi T \frac{\partial v}{\partial x} = \frac{\partial}{\partial x}\left(k \frac{\partial T}{\partial x} \right) + \frac{A_h}{A_c}\frac{2 f \rho |v| v^2}{D_h} + \dot{q}''' \tag{3}$$

where the meaning of most symbols is standard (see the list of symbols in App. 3) and we have defined the following averaged heat capacities:

$$\hat{C}_t = \hat{C}_v + \frac{\rho_c}{\rho} C_c$$

$$\hat{C}_v = \frac{A_h}{A_c} C_v \quad .$$

The Joule heating term $\dot{q}'''$ is zero everywhere except in the quench region where the temperature is greater than the so called *current sharing temperature* T_{cs}. The above model gives a very good approximation to the propagation of a fully developed quench in a superconducting cable [4]. In their original form the equations describing a quench are strongly dominated by the hyperbolic character of the Euler equations, and in particular the heat convection term. We took care to maintain this feature (the second term on the l.h.s of Eq. (3)) in the simplification process leading to the model above.

To present an example of a quench initiation and propagation and the difficulties associated with the numerical solution, we have considered conditions similar to those of an experiment performed by Ando et al. [6]. In this experiment an external heater was used to rapidly initiate a quench at the center of a superconducting cable of 26 m length. The cable characteristics and operation conditions used as input for the simulation are reported in Tab. I. Note that we have artificially modified the cable characteristics, in particular decreasing the thermal conduction in the cable, in order to more clearly highlight the numerical difficulties.

A reference simulation, solving the system of Eqs. (1)-(3), was performed using a standard, adaptive second order accurate algorithm based on central differencing in space and time (see App. 1 and Ref. [5]) and taking care to reach numerically converged results. We show in Fig. 1 the temperature profiles at different times (solid lines). The normal zone can be identified there as the region where the temperature is above the current sharing limit T_{cs}=5 K. Note that symmetry around the central point, located at *x=0*, has been assumed, and only a detail of half of the length has been

plotted. In the normal region Joule heating causes the temperature to increase, accompanied by the expansion of the compressible helium in this region. The heated helium stream expands through the portions of the cable length which is still superconducting. Through heat exchange between the high temperature helium and the superconductor the normal zone propagates along the cable.

The normal zone propagation for this case is illustrated in Fig. 2 (solid curve), where the location of the normal front X_q is plotted as a function of time. This location represents a moving boundary layer in the problem, determined implicitly by the evolution of the temperature profile, and according to the condition:

$$T\left(X_q\right) = T_{cs}\,.$$

The difficulties associated with the numerical simulation of quench propagation are demonstrated using a first order accurate upwind finite difference algorithm with implicit time stepping and fixed time and space steps (see again App. 1 for details on the algorithm). In Fig. 1 we compare the temperature profiles obtained by this method at typical practical space and time steps of 1 cm and 0.1 ms, respectively, to those of the converged solution. While the accuracy on the maximum temperature at $x = 0$ is acceptable, it is evident that the normal zone propagation is not. The temperature profile at the front is strongly smeared, and the normal zone propagation is much more rapid than for the converged results.

The convergence of the first order algorithm can also be seen in Fig. 2, where the location of the normal front is plotted as a function of time for different values of the space step Δx and for a fixed time step of 0.1 ms. These results are compared with the *converged* solution obtained by using the second order method (solid line). Notice the large error introduced by the first order algorithm, leading to an artificial acceleration of the quench front. Such explosive propagation of the quench is only physically possible during a "Thermal Hydraulic Quenchback" (THQB), a situation in which the frictional heating ahead of the normal zone can cause the helium temperature to go above T_{cs}, resulting in a very different quench propagation mechanism [7]. The numerically non-converged solution shows a similar behavior as the physical process of the THQB. For this reason, we use the term Numerical Quenchback (NQB) to characterize a non-converged solution of the governing model.

In Fig. 3 we plot the error on the normal front location as a function of $1/\Delta x$ and for a fixed time step of 0.1 ms. The error is defined as the difference between the solution obtained by the first order algorithm and the converged solution obtained with the second order algorithm. The convergence rate of the first order method is unexpectedly slow. In fact, the first order method appears to converge with a rate close to 0.5, instead of the expected value of 1. Similar results can be obtained for the second order algorithm, where convergence rates slower than the expected value of 2 are observed (typical convergence rates are between 1 and 1.5).

The problem presented here is of practical interest as it implies that in order to obtain accurate solutions of quench evolution, extremely small space and time step are required. Typical conductor lengths for superconducting coils range between 100 m to 1 km, and quench time scales are of the order of 10 s. Uniform space and time mesh sizes as those used in the previous example would lead to astronomic CPU time.

Mesh adaptivity has been used to more efficiently solve the propagation of quench [4,5], which still remains a heavy computational task. However, even when higher order computational algorithms are used, a complete space and time convergence analysis is a tedious and time consuming task. It is therefore of interest to identify the causes of the low convergence rate, so that a suitable and efficient error control can be implemented to qualify the solution. Loss of accuracy on the position of the normal front also results in extremely low accuracy of other important quantities of interest such as the maximum helium pressure rise during the quench. Here, we will concentrate on the normal front and its velocity as general indicators for the quality of the solution. The influence of the normal length and its propagation on all other variables is discussed in Ref. [4].

We will show that the low convergence rate is a feature of the non-linearity of the governing system of equations and the motion of the boundary layer at the location of the quench front. Specifically, we first develop a "model problem" that maintains all of the essential physics, but is easier to track analytically. Furthermore, we show that indeed the model problem reproduces the features of slow convergence rate and the rapid quench front acceleration observed in the numerically non-converged solutions of the more complete model. Based on the results of the analytical study we show in detail the *physics* underlying the NQB process. Finally, an analytic relation is presented for the error introduced by the numerical scheme on the normal front location, based on which the space and time steps can be chosen to avoid NQB. The study will be based on the upwind (first order) and central differences (second order) schemes already introduced. These are not the *optimal* choice for convection dominated problems, as it can be demonstrated in the context of finite elements [8]. Nevertheless, they have well established discretization properties that we will use to derive more general conclusions on the effect of numerical errors on quench propagation.

2. Model problem definition and analytical solution

The set of Eqs. (1)-(3) describing quench in CICC are cumbersome and difficult to solve analytically, even with the simplifying assumption of constant material properties. The main difficulty lies in the non-linear coupling of the equations. To simplify the analysis we define here a model problem that includes the important feature of the moving boundary layer at the quench front. Furthermore, all of the difficulties observed in the numerical solution of Eqs. (1)-(3) are also encountered in solving the model problem.

We start by assuming that compressibility and friction phenomena can be neglected, and we drop the contribution of heat conduction in the energy balance. Furthermore, we assume that the dominant heat capacity is that of helium (i.e. $\hat{C}_t = \hat{C}_v = C$). This is a well justified approximation in the region close, and ahead of the normal front where the temperatures are low. On the other hand in the normal zone the helium depletion during a real quench is such that the dominant heat capacity in this region is that of the conductor. Also, in this region both the heat production and the heat capacity increase rapidly with temperature, changing by orders of magnitude according to the temperature dependence of the specific heat and that of the electrical resistivity. However, the ratio of the heat source term to the heat capacity varies by a

much smaller factor and can be assumed to be constant for the purposes of our analysis.

With the above simplifying assumptions, Eqs. (1)-(3) become:

$$\frac{\partial \rho}{\partial t} + \frac{\partial \rho v}{\partial x} = 0 \tag{4}$$

$$p = p_0 \tag{5}$$

$$\frac{\partial T}{\partial t} + v\frac{\partial T}{\partial x} = QH\left(T - T_{cs}\right) \tag{6}$$

where $Q = \frac{\dot{q}'''}{\rho C}$ is the ratio of heat generation to the heat capacity and $H(T\text{-}T_{cs})$ is the Heavyside step function. As discussed above, we consider Q to be a constant. The problem is defined over the domains $x \in \Re^+$ and $t \in \Re^+$.

This simplified form evidences the convection term in the energy equation (Eq. (6)), where we notice that in our case the velocity is not independent of temperature, as generally assumed in convection dominated heat transport, but is coupled to the temperature profile through the continuity equation (Eq. (4)). To allow further analytic treatment of the problem, we now make the additional assumption that the fluid behaves as an ideal gas, i.e.

$$p = \rho RT \tag{7}$$

where R is the gas constant of helium. The model problem specification is now complete. The initial conditions are given by:

$T(t=0)=T_{cs}^{+}$ for $0 < x \le X_{q0}$
$T(t=0)=T_0<T_{cs}$ for $x > X_{q0}$,

where X_{q0} is the location of the quench front at time $t=0$. The symmetry boundary conditions at the center of the cable are given by:

$$\left.\frac{\partial T}{\partial x}\right|_{x=0} = 0$$

$$v(0,t) = 0 \quad .$$

Equations (5) and (7) give a relation between the gas density and its temperature. By appropriately adding Eqs. (4) and (6) a single relation is obtained between v and T:

$$T\frac{\partial v}{\partial x} = QH\left(T - T_{cs}\right) \tag{8}$$

which shows, as expected, that because of neglecting inertia the fluid velocity responds immediately to the changes in the fluid temperature. Equation (8) can now be used to eliminate the velocity.

Having eliminated both the density and velocity in terms of temperature, it is now straightforward to find an analytical solution for the temperature profile. Since the model contains no diffusion, the quench propagates with the heating-driven expansion of the helium bubble contained in the initial normal region. The temperature profile is a step function at the location of the moving front. Ahead of the front the temperature is equal to the unperturbed temperature T_0, while behind the front the profile is uniform and is given by:

$$T\left(x\,;\,x \le X_q\right) = T_o + Qt \qquad (9).$$

The quench propagation speed is then calculated from Eq. (8), integrating the temperature profile. The normal front speed is given by:

$$V_q^{an} = \frac{Q}{T_{cs}} X_{qo} \qquad (10)$$

which is constant in time. Here, we use the superscript *"an"* to indicate the exact analytic solution of the model problem. Observe that the value of the constant is determined by the heating rate, material properties, and depends on the initial normal length X_{q0}. Also note that:

$$V_q^{an} = v\left(x = X_q\,,t\right)$$

the analytical propagation speed is identical to the fluid velocity at the front. The instantaneous position of the normal front is finally obtained by integrating Eq. (10), and is given by:

$$X_q^{an} = X_{qo}\left(1 + \frac{Q}{T_{cs}} t\right) \qquad (11).$$

3. Numerical solution of the model problem

Consider the model problem defined in the previous section. Here we demonstrate the effect of numerical errors on the quench propagation velocity. For the numerical solution of the model problem we have used the two algorithms introduced earlier with global first and second order accuracy in time and space, respectively.

In Fig. 4(a) we present the temperature profile as obtained by the first and second order schemes using the input data of Tab. 2. The solid line in this figure represents the analytic solution obtained in the previous section. Observe that the temperature distribution obtained by both schemes clearly shows the *pathology* of non-convergence. Namely both algorithms show a smeared front and an accelerating normal zone. Figures 4(b) and 4(c) show respectively the helium density and velocity profiles for this case. Again, the non-converged solutions show a much different behavior with almost an order of magnitude larger flow velocities. Finally, in Fig. 5 we present the normal front location (symbols) as a function of time. The exact analytical solution (solid straight line) is also shown for comparison.

Let us try to understand the non-convergence behavior of the numerical schemes. As shown in App. 1 any numerical scheme accurate to order *n-1*, including those used here, has an associated error that appears in the equivalent differential equation [9], given by:

$$\varepsilon = \alpha_n \frac{\partial^n T}{\partial x^n} + o\left(\Delta x^n, \Delta t^n\right)$$

where the parameter α_n is proportional to a combination of the $(n\text{-}1)^{th}$ power of the space and time steps. Thus, a first order accurate scheme introduces a numerical diffusion, while a second order scheme results in numerical dispersion. This well known behavior appears in the different temperature profiles generated by the first and second order schemes (see Fig. 4(a)), where the former smears the sharp front and the latter produces oscillations at the normal front. However, excessive diffusion and dispersion alone cannot explain the exponential front acceleration.

As shown in Appendix 2, the numerical error also results in an *additional* propagation velocity. In the case of the model problem the additional velocity V_{ad} associated with the numerical discretization can be computed *a priori* using the equivalent differential equation of the scheme. In particular the following asymptotic expressions for the two schemes considered here are obtained in App. 2:

first order algorithm:

$$V_{ad} = \sqrt{\frac{Q\left|\alpha_2\right|}{\left(T_{cs} - T_0\right)}} \tag{12}$$

where:

$$\alpha_2 = -\frac{v}{2}\left(\Delta x + v\Delta t\right) \tag{13}$$

second order algorithm:

$$V_{ad} = \left(\left(\frac{Q}{2\left(T_{cs} - T_0\right)}\right)^2 \alpha_3\right)^{1/3} \tag{14}$$

where:

$$\alpha_3 = \frac{v}{6}\left(\Delta x^2 + \frac{v^2 \Delta t^2}{2}\right) \tag{15}.$$

Note that the additional speed introduced by the numerical scheme is constant in both cases.

In the case of the first order scheme it is possible to verify that indeed the addition of the numerical diffusion causes the problem to diverge. We have solved the equivalent differential equation for the first order scheme - including the numerical error given by Eq. (13) above - using the second order scheme. We have thus simulated the asymptotic behavior of the first order scheme including its first truncation term. The results of this study are reported in Fig. 5 (dotted lines) where they are compared to the actual performance of the first order scheme (symbols). Note the good agreement between the two solutions, which converge asymptotically towards the same behavior (at the smallest mesh spacing the dashed curve cannot be distinguished from the symbols). This proves that the front acceleration is caused by the numerical error, at least in the first order accurate scheme.

The explanation for this fact lies in the coupled nature of the system of equations under consideration. The constant propagation speed V_q for the model problem is obtained only when the total helium mass in the normal zone is a constant. In the case of the numerical solution the additional front velocity V_{ad} causes the front to advance the helium expulsion and to engulf new helium mass in the normal zone. To satisfy the constant pressure condition, the fluid expulsion velocity from the normal zone v must therefore continuously increase, causing an acceleration of the quench front.

The front propagation velocity for the equivalent differential equation of the numerical scheme is given by the sum of the helium expulsion velocity at the front location and the additional speed of numerical origin:

$$V_q^{num} = v^{num} + V_{ad} \tag{16}$$

where the superscript *"num"* is used to denote the solution of the equivalent differential equation of the numerical scheme. We already know V_{ad} , hence to solve Eq. (16) we need next to find the helium expulsion velocity v^{num}. This can be done by approximating the temperature profile in the normal region, just behind the quench front, using a piece wise linear profile. Using this approximate profile in Eq. (8) we obtain the following expression for the expulsion velocity:

$$v^{num} = V_q^{an} + \frac{X_q^{num} - X_q^{an}}{t} \log\left(1 + \frac{Q}{T_{cs}} t\right) \tag{17}$$

where V_q^{an} and X_q^{an} are given by Eqs.(10) and (11), respectively. The system of Eqs. (16) and (17) is closed by the relation between the front position and its velocity:

$$V_q^{num} = \frac{dX_q^{num}}{dt} .$$

It is more convenient to solve Eqs. (16) and (17) in terms of the relative error on the normal front location ε, defined as:

$$\varepsilon = \frac{X_q^{num} - X_q^{an}}{X_q^{an}} \quad .$$

Equations (16) and (17) can be combined and rewritten in terms of ε as follows:

$$\frac{d\varepsilon}{dt} = \frac{1}{X_q^{an}} \left\{ V_{ad} + V_q^{an} \varepsilon \left[1 + \log\left(1 + \frac{Q}{T_{cs}} t \right) \right] \right\} \tag{18}$$

This is an ODE for ε with the initial condition $\varepsilon(0) = 0$. If we retain only the dominant terms at large times we obtain the following approximation:

$$\frac{d\varepsilon}{dt} \approx \frac{\varepsilon}{t} \log\left(\frac{Q}{T_{cs}} t \right) \tag{19}$$

with the solution:

$$\varepsilon = \varepsilon_0 e^{\frac{1}{2}\left[\log\left(Qt/T_{cs}\right)\right]^2} \tag{20}.$$

The constant ε_0 must be determined by matching Eq. (20) to the solution of Eq. (18) in the limit $t \to 0$. After a straight forward calculation it can be shown that:

$$\varepsilon_0 = \frac{V_{ad}}{V_q^{an}} .$$

Now, recalling the definition of ε, we obtain from Eq. (20) an analytic expression for the position of the normal front which includes the effects of the numerical discretization error:

$$X_q^{num} = X_q^{an} + V_{ad} t \, e^{\frac{1}{2}\left[\log\left(Qt/T_{cs}\right)\right]^2} \tag{21}.$$

This is the desired result. Note the exponentially growing term in Eq. (21). That is, V_q^{num} does not simply equal to the sum $V_q^{an} + V_{ad}$ as would be obtained from the analysis of the numerical error in the linear case (i.e. neglecting the coupling with the continuity balance). This would result in an error term which increases linearly in time. What we have found is a much more severe situation as can be seen in Eq. (20). Three contributing factors result in the rapidly growing error term appearing in this equation: 1) the constant multiplying the error term V_{ad} is a direct consequence of the numerical discretization error, 2) the term appearing in the exponential is directly related to the moving source term, and more specifically the moving step function located at the leading edge of the source term, and finally, 3) the fact that the error term is a non-linear function of time is attributed to the non-linearity of the model problem.

The estimated front position given by Eq. (21) has been computed for the case of the model problem, and is reported in Fig. 5 (dashed lines) for comparison with the

results of the numerical simulation. The agreement between the dashed lines and the symbols is good. In addition, the results of the numerical simulation and its analytical approximation get closer as the limit of small Δx is approached (the error estimates for the numerical schemes, Eqs. (13) and (15), are only accurate in the limit $\Delta x \to 0$).

In summary, we have shown that Eq. (21) approximates well the behavior of the equivalent differential equation of the numerical scheme. We would like to reiterate that Eq. (21) properly takes into account the *physics* behind the numerical solution of the model problem, namely the interplay of the quench front advancement in time and the fluid mass expulsion from the quench region. The method developed is general, and can be applied to an arbitrary solution scheme once the additional front speed V_{ad} originated by the truncation error is known.

4. Numerical convergence criteria for quench simulation

The study of the numerical solution of the model problem performed in the previous section has given considerable insight on the effect of numerical errors. These appear as an additional front propagation speed which, in turn, is at the origin of the non-physical and rapid front acceleration. It can be shown that the conditions of the model problem are analogous to the *small pressure rise* limit in the propagation of a real quench [4]. Therefore from the point of view of the accuracy of the physics modelling we expect that the conclusions reached in the previous section also apply (at least approximately) to more realistic quench scenarios represented by Eqs. (1)-(3).

From the point of view of the numerical schemes used, we already remarked that both schemes (upwind and central differencing) are not the choice of reference for convection dominated problems. Several algorithms have been developed in the past years, generally applicable to compressible and incompressible, viscous and inviscid flow (see for instance Refs. [10-13] for some finite volume and finite element algorithms and the general overview in Ref. [9]). Most of these methods are explicit for reasons of computational efficiency. Some taylored artificial diffusion, high order dispersion or dissipation is generally added to stabilize high frequency modes. The addition is either made based on operating experience on the algorithm [9,10], or can be justified in the frame of the general derivation of the method [11-13], and is usually specific to the simulation of the flow. Only more recently generally applicable, well stabilized methods are being proposed [14], potentially capable of treating very different situations in a consistent frame.

In fact in the most general solution of quench propagation [5], as discussed in the introduction, we are confronted with strong thermal coupling between the superconducting cable and helium making the problem intrinsically stiff. Furthermore material properties and source terms are highly non-linear. Finally, a strong convection term is present only in the mass and energy balances, while the other equations are dominated by diffusion or source terms. To deal efficiently with these features low order, flexible, adaptive implicit methods have been preferred so far [2-5,15]. Indeed, the schemes used at present for this purpose have at most second order accuracy, and therefore the study based here on upwind and central differences is directly applicable.

In order to obtain a simple numerical convergence criteria for the problem of quench propagation we propose to impose a tolerance on the error in the location of the normal front at the end of the simulation. That is, we must have

$$\varepsilon\,(t=t_{max}) < \varepsilon_{max},$$

where ε_{max} is the specified error tolerance, t_{max} is the time scale of interest during the numerical simulation, and ε is given by Eq. (20). This criteria can easily be recast in a relation that involves V_{ad}, given by:

$$\frac{V_{ad}}{V_q} \le \varepsilon_{\max} e^{-\frac{1}{2}[\log(T_{\max}/T_{cs})]^2} \tag{22}$$

where we have replaced the product $Q\ t$ by T_{max} which is the maximum (hot-spot) temperature reached during the quench and is usually a specified allowable for the operation of a coil. This is the desired result for the convergence criteria of the numerical solution. Note that V_{ad} is directly related to the space and time steps used in the numerical discretization (see App. 2).

In order to demonstrate how Eq. (22) can be used to appropriately choose Δx and Δt, consider a typical quench with V_q = 10 m/s, T_0 = 5 K, T_{cs} = 10 K, Q = 10 K/s and T_{max} = 100 K. Setting for instance a 5 % tolerance on the front location (ε_{max} = 0.05) we find that the limit condition on the additional quench speed of numerical origin is V_{ad} < 0.035 m/s. Depending on the scheme we can now determine from Eqs. (12) and (14) the space and time step that would result in such an additional front speed. We can assume that the helium velocity is approximately equal to the propagation speed, i.e. $v \approx 10$ m/s. If we suppose in addition to operate at unit Courant number, i.e. $\Delta t = \Delta x/v$, we obtain that the first order scheme must have $\Delta x < 0.1$ mm and $\Delta t < 10$ μs, obtained using Eqs. (12) and (13). In the case of the second order accurate algorithm, using Eqs. (14) and 15 we find $\Delta x < 5$ mm and $\Delta t < 0.5$ ms. From our direct experience [15], this is in fact the range of mesh sizes that are required in order to obtain a converged solution of the quench process.

5. Conclusions

In this paper we have discussed and analyzed the process of NQB observed in the numerical solution of quench propagation in superconducting magnets. Specifically, we have shown that exponentially growing error terms are present in the numerical solution of the normal front position. The cause of such unstable solutions is shown to be due to the discretization error, the nonlinear nature of the model, and the boundary layer motion at the quench front. Analytic relations are presented to minimize NQB when attempting to numerically solve the quench problem.

References

[1] M. Wilson, *Superconducting Magnets*, Clarendon Press, Oxford, 1983.

[2] J.K. Hoffer, *The Initiation and Propagation of Normal Zones in a Force-cooled Tubular Superconductor*, IEEE Trans. Mag., **15**, 1, 331-336, 1979.

[3] V.D. Arp, *Stability and Thermal Quenches in Force-cooled Superconducting Cables*, Proc. of 1980 Superconducting MHD Magnet Design Conference, MIT, 142-157, 1980.

[4] A. Shajii, J.P. Freidberg, *Quench in Superconducting Magnets. I. Model and Implementation*, J. Appl. Phys., **76**, 5, 3149-3158, 1994. *II. Analytic Solution*, J. Appl. Phys., **76**, 5, 3159-3171, 1994.

[5] L. Bottura, *A Numerical Model for the Simulation of Quench in the ITER Magnets*, Jour. Comp. Phys., **125**, 26-41, 1996.

[6] T. Ando, M. Nishi, T. Kato, J. Yoshida, N. Itoh, S. Shimamoto, *Propagation Velocity of the Normal Zone in a Cable-in-Conduit Conductor*, Adv. Cryo. Eng., **35**, 701-708, 1990

[7] A. Shajii, J.P. Freidberg, *Theory of Thermal Hydraulic Quenchback*, Int. J. Heat Mass Transfer, **39**, 3, 491-501, 1996

[8] O.C. Zienkiewicz, R.L. Taylor, *The Finite Element Method*, Vol. 2, McGRAW-Hill (UK), 1991

[9] C. Hirsch, *Numerical Computation of Internal and External Flows*, J. Wiley & Sons, 1988

[10] A. Jameson, W. Schmidt, E. Turkel, *Numerical Simulation of the Euler Equations by Finite Volume Methods using Runge-Kutte Time Stepping Schemes*, AIAA, Paper 81-12-59, AIAA 5th Comp. Fluid Dynamics Conf., 1981.

[11] A.N. Brooks, T.J.R. Hughes, *Streamline upwind/Petrov-Galerkin Formulations for Convective Dominated Flows with Particular Emphasis on the Incompressible Navier-Stokes Equations*, Comp. Meth. Appl. Mech. Eng., **32**, 199-259, 1982

[12] J. Peraire, J. Peiro, L. Formaggia, K. Morgan, O.C. Zienkiewicz, *Finite Element Euler Computations in 3-Dimensions*, Int. Jour. Num. Meth. Eng., **26**, 2135-2159, 1989

[13] C. Johnson, U. Nävert, J. Pitkäranta, *Finite Element Method for Linear Hyperbolic Problems*, Comp. Meth. Appl. Mech. Eng., **45**, 285-312, 1984

[14] L.P. Franca, C. Farha, M. Lesoinne, A. Russo, *Unusual Stabilized Finite Element Methods and Residual Free Bubbles*, Int. Jour. Num. Meth. Eng., **27**, 159-168, 1998

[15] L. Bottura, A. Shajii, *On the Numerical Studies of Quench in Cable-in-Conduit Conductors*, IEEE Trans. Appl. Sup., **5**, 2, 495-498, 1995

Table 1. Data for the quench propagation experiment of Sect. 1. The conductor and operating conditions are similar to the experiment of Ando et al. [6]. Particular parameters (marked by an asterisk) have been adapted to show higher sensitivity to the numerical solution.

Conductor geometry

Strand diameter (mm)	0.98
Number of strands	18
NbTi cross section (mm^2)	3.4
Copper cross section (mm^2)	10.2
Helium cross section (mm^2)	13.3
Hydraulic diameter (m)	$0.069^{(*)}$
Copper resistivity (Ωm)	6×10^{-10}
Copper thermal conductivity (W/m K)	$1^{(*)}$

Operating and critical conditions

Magnetic field (T)	7
Temperature (K)	4.2
Pressure (MPa)	1.0
Mass flow (g/s)	0.0
Critical temperature (K)	6.24
Critical current (kA)	3.0
Operating current (kA)	1.8
Current sharing temperature (K)	≈5

Table 2. Parameters used in the numerical solutions of the model problem.

Initial temperature T_0	1.0
Current sharing temperature T_{cs}	1.25
heating rate ratio $Q = \dot{q}''' / \rho C$	1
Initial normal length X_{q0}	1.0
Analytical quench velocity V_q	0.8

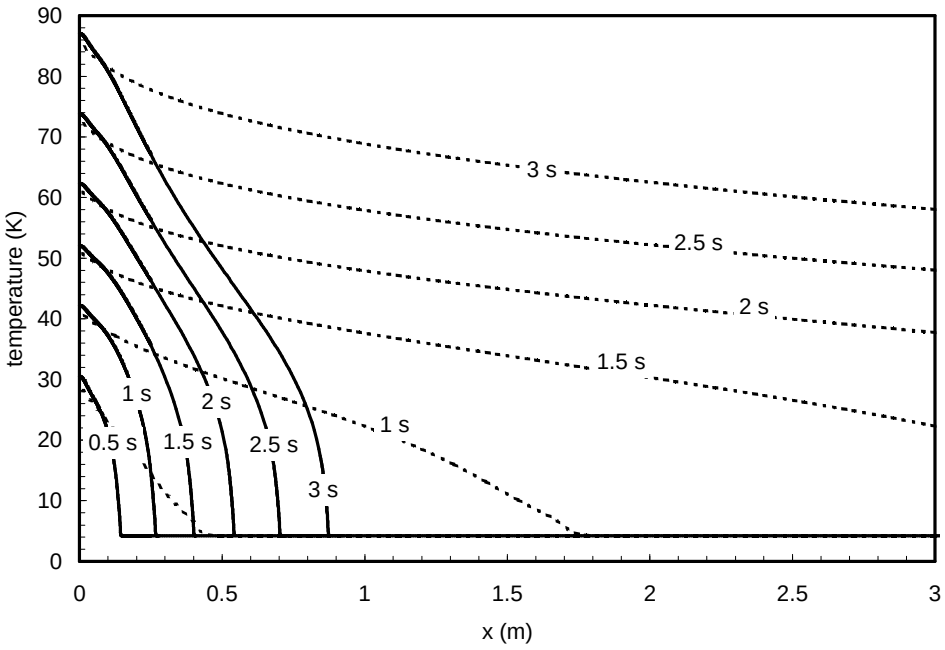

Figure 1. Temperature profiles computed at different times (indicated on the curves) for the quench evolution in the case defined in Tab. I. The solid line represents the converged solution obtained with a second order algorithm and is compared to non-converged profiles (dashed lines) obtained with a first order algorithm on a fixed mesh size Δx of 1.25×10^{-2} m, time step Δt of 0.1×10^{-3} s.

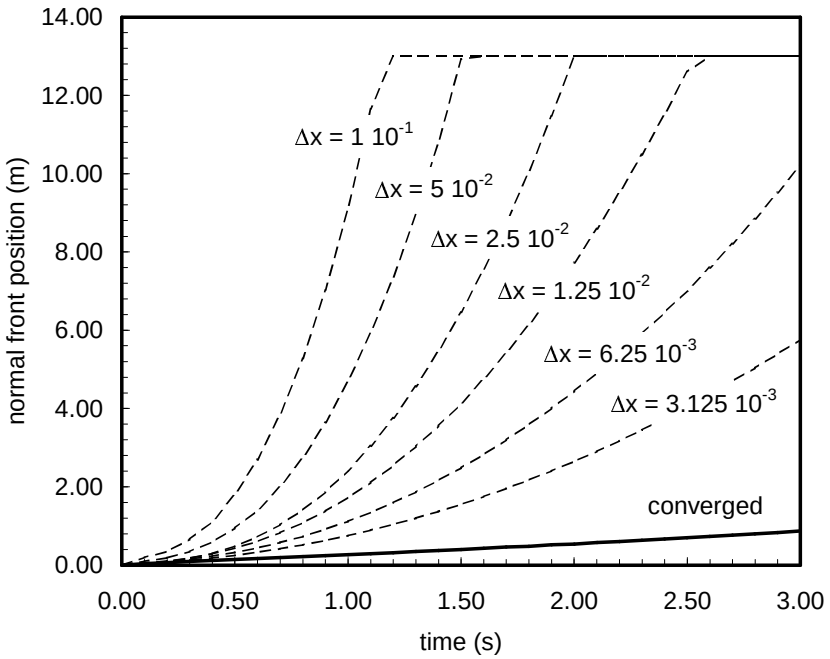

Figure 2. Normal length evolution in the case defined in Tab. I. The converged solution obtained with a second order algorithm is the solid line, and is compared to the non-converged profiles obtained with a first order algorithm (fixed mesh spacing as indicated on the dashed lines, time step Δt of 0.1×10^{-3})

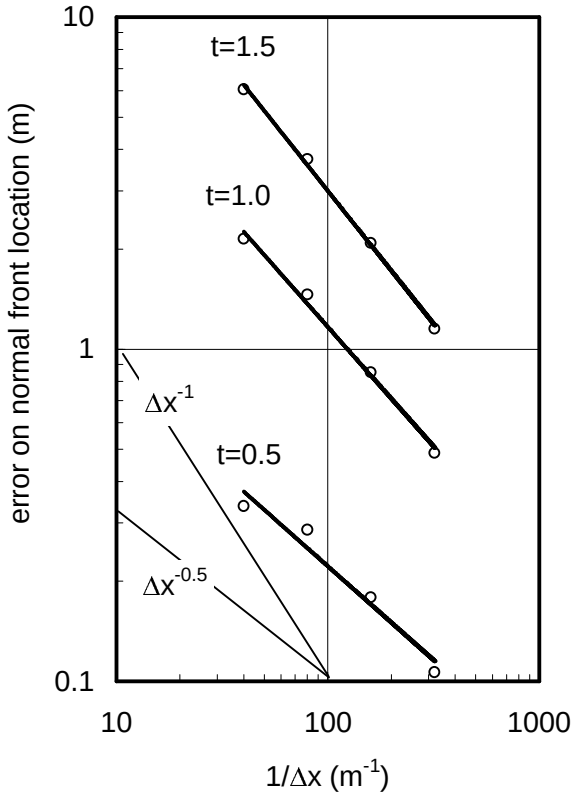

Figure 3. Error in the normal length evolution in the case defined in Tab. I for the first order algorithm, at different times as indicated. The converged solution obtained with a second order algorithm is used as *exact* solution to compute the error. The slopes for convergence rates of 0.5 and 1 are indicated by the thin lines.

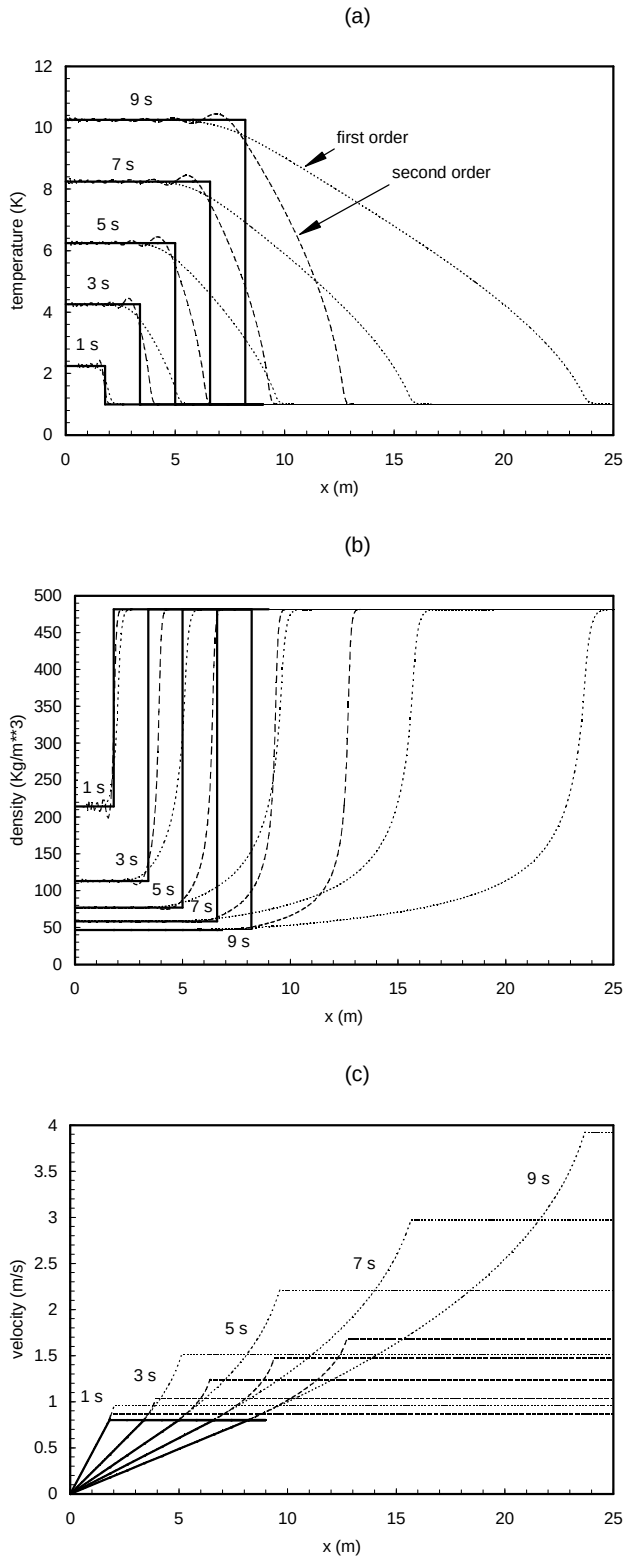

Figure 4. Temperature (a), density (b) and velocity (c) distributions at different times (indicated on the curves) computed with the first (dotted lines) and second (dashed lines) order schemes for the conditions of the model problem taking a space step Δx of 5×10^{-2} and a time step Δt of 5×10^{-4}. The exact, analytical solution is also shown for comparison (solid lines).

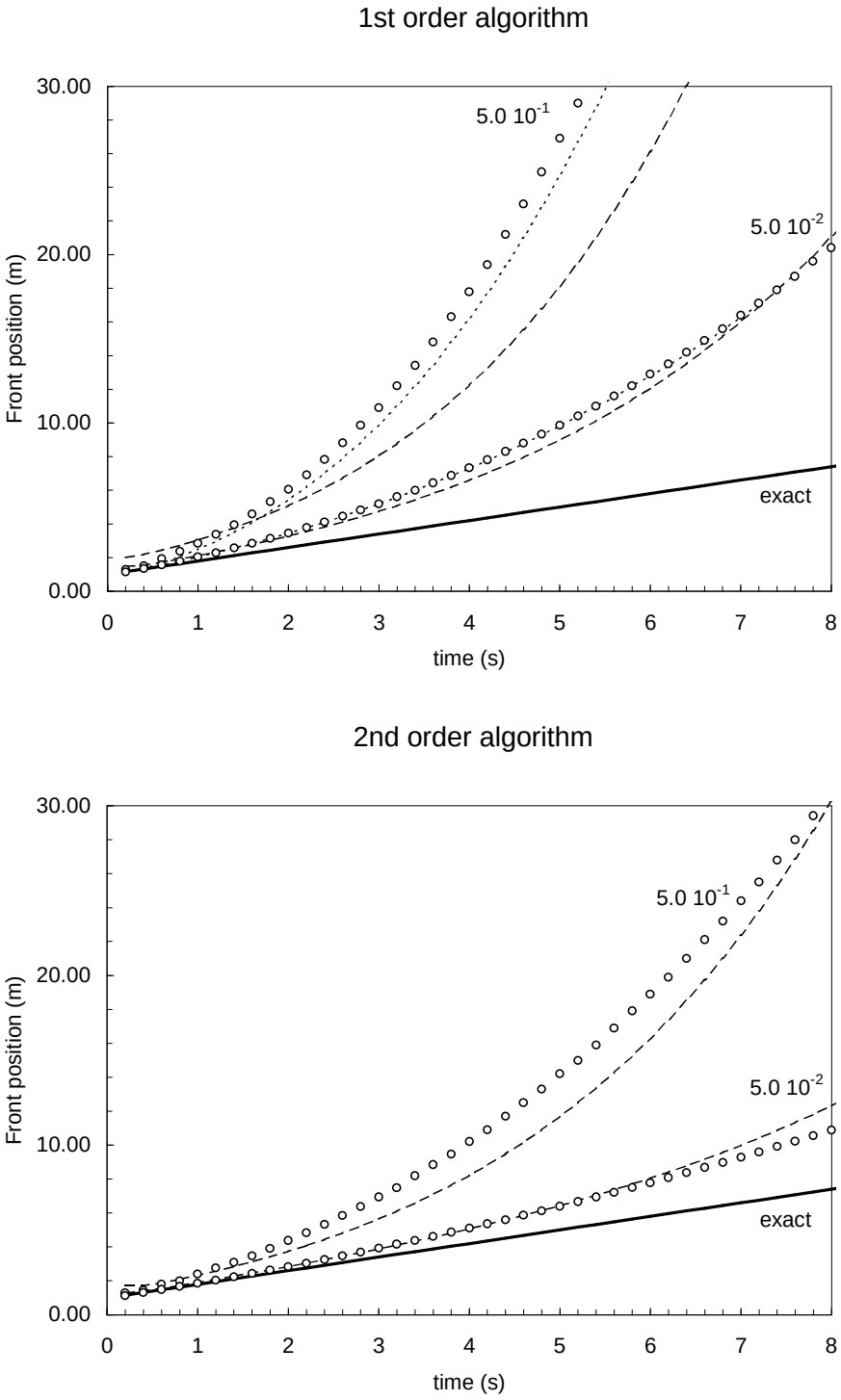

Figure 5. Total normal length (symbols) computed with the first (top) and second (bottom) order schemes for the conditions of the model problem taking the space step Δx as a parameter (indicated on the curves) and a time step Δt of 5×10^{-3}. The exact, analytical solution is also shown for comparison. The dotted lines for the first order scheme are results from the numerical solution of the equivalent differential equation using a second order algorithm. The dashed line is the analytic approximation given by Eq. (16).

Appendix 1 Space and time discretization and numerical error

Equations (1)-(3) form a non-linear hyperbolic system. Apart from non-linearities, the main features of such a system are conveniently studied using the simple scalar equation:

$$\frac{\partial T}{\partial t} + v\frac{\partial T}{\partial x} = 0 \qquad (1.1).$$

which has the same structure as Eq. (6), defining the model problem. Here, we consider standard first and second order accurate algorithms[9] with the following difference equations (subscripts indicate mesh points in space and superscripts stand for time):

first order method implicit in time:

$$\frac{T_i^{n+1} - T_i^n}{\Delta t} + v\frac{T_i^{n+1} - T_{i-1}^{n+1}}{\Delta x} = 0 \qquad (1.2)$$

second order method implicit in time:

$$\frac{T_i^{n+1} - T_i^n}{\Delta t} + \frac{v}{2}\frac{T_{i+1}^n - T_{i-1}^n}{2\Delta x} + \frac{v}{2}\frac{T_{i+1}^{n+1} - T_{i-1}^{n+1}}{2\Delta x} = 0 \qquad (1.3).$$

we show here for completeness the errors associated with the above approximations as they can be obtained using the equivalent differential equation of the schemes[9]. At a given time step we have:

$$T^{n+1} = T^n + \Delta t\frac{\partial T}{\partial t}\bigg|^n + \frac{\Delta t^2}{2}\frac{\partial^2 T}{\partial t^2}\bigg|^n + \frac{\Delta t^3}{6}\frac{\partial^3 T}{\partial t^3}\bigg|^n + o\left(\Delta t^4\right)$$

and at a given mesh point we can write the following expressions:

$$T_{i-1} = T_i - \Delta x\frac{\partial T}{\partial x}\bigg|_i + \frac{\Delta x^2}{2}\frac{\partial^2 T}{\partial x^2}\bigg|_i - \frac{\Delta x^3}{6}\frac{\partial^3 T}{\partial x^3}\bigg|_i + o\left(\Delta x^4\right)$$

$$T_{i+1} = T_i + \Delta x\frac{\partial T}{\partial x}\bigg|_i + \frac{\Delta x^2}{2}\frac{\partial^2 T}{\partial x^2}\bigg|_i + \frac{\Delta x^3}{6}\frac{\partial^3 T}{\partial x^3}\bigg|_i + o\left(\Delta x^4\right).$$

If we insert the above relations in the Eqs. (1.2) and (1.3) we find:

first order method:

$$\frac{\partial T}{\partial t} + v\frac{\partial T}{\partial x} - \frac{v}{2}\left(\Delta x + v\Delta t\right)\frac{\partial^2 T}{\partial x^2} + o\left(\Delta x^2\right)\frac{\partial^3 T}{\partial x^3} = 0 \qquad (1.4)$$

second order method:

$$\frac{\partial T}{\partial t} + v\frac{\partial T}{\partial x} + \frac{v}{6}\left(\Delta x^2 + \frac{v^2\Delta t^2}{2}\right)\frac{\partial^3 T}{\partial x^3} + o\left(\Delta x^3\right)\frac{\partial^4 T}{\partial x^4} = 0 \qquad (1.5).$$

where the following identities have been used in deriving Eqs. (1.4) and (1.5):

$$\frac{\partial T}{\partial t} = -v\frac{\partial T}{\partial x}$$
$$\frac{\partial^2 T}{\partial t^2} = v^2\frac{\partial^2 T}{\partial x^2}$$
$$\frac{\partial^3 T}{\partial t^3} = -v^3\frac{\partial^3 T}{\partial x^3}$$

The last two terms on the left hand side of the equivalent differential equations represent the error introduced by the numerical discretization. For both methods the solution of the discretized form of Eq. (1.1) is thus equivalent to the exact solution of the following modified problem:

$$\frac{\partial T}{\partial t} + v\frac{\partial T}{\partial x} + \alpha_n\frac{\partial^n T}{\partial x^n} = 0 \qquad (1.6)$$

where for the first order accurate method:

$$n = 2$$
$$\alpha_2 = -\frac{v}{2}\left(\Delta x + v\Delta t\right)$$

and for the second order accurate method:

$$n = 3$$
$$\alpha_3 = \frac{v}{6}\left(\Delta x^2 + \frac{v^2\Delta t^2}{2}\right)$$

Appendix 2 Calculation of additional front velocity for the numerical solutions of the model problem

Consider the governing equation for temperature in the model problem:

$$\frac{\partial T}{\partial t} + v\frac{\partial T}{\partial x} = QH\left(T - T_{cs}\right) \tag{2.1}$$

By virtue of the results of App. 1, any numerical solution of (2.1) is equivalent to the integration of a modified equation of the following form:

$$\frac{\partial T}{\partial t} + v\frac{\partial T}{\partial x} + \alpha_n \frac{\partial^n T}{\partial x^n} = QH\left(T - T_{cs}\right) \tag{2.2}$$

where the leading order numerical error has been written as a space derivative contribution of order n (n-*1* is the global order of accuracy of the method). The coefficient α_n will be in general related to the n-*1* power of the space and time steps used in the discretization.

The exact solution of Eq. (2.2), and therefore a numerical approximation to Eq. (2.1) produces an additional propagation speed for the quench front (V_{ad}). To prove this statement consider the following coordinate transformation:

$$\xi = x - V_q t$$

The change of coordinates in Eq. (2.2) gives the following result:

$$\frac{\partial T}{\partial t} + \left(v - V_q\right)\frac{\partial T}{\partial \xi} + \alpha_n \frac{\partial^n T}{\partial \xi^n} = \frac{\dot{q}'''}{\rho C} H\left(-\xi\right) \tag{2.3}$$

We now make the assumption that asymptotic behavior is reached, and therefore in the immediate vicinity of the quench front the temperature profile in the moving reference frame does not change in time. This justifies neglecting the time derivative term in Eq. (2.3). Thus, we have

$$-V_{ad}\frac{\partial T}{\partial \xi} + \alpha_n \frac{\partial^n T}{\partial \xi^n} = 0 \quad for \quad \xi \geq 0 \tag{2.4}$$

$$-V_{ad}\frac{\partial T}{\partial \xi} + \alpha_n \frac{\partial^n T}{\partial \xi^n} = \frac{\dot{q}'''}{\rho C} \quad for \quad \xi < 0 \tag{2.5}$$

where by definition X_q. The solution of these equations, and the jump conditions on the temperature and its derivatives at the quench front are specific to the particular value of n. Here, we present the results for n=2 (first order accurate algorithm) and n=3 (second order accurate algorithm).

First order accurate algorithm (n=2).

In this case the general solution of the homogeneous Eq. (2.4) is:

$$T = A_1 + A_2 e^{\frac{V_{ad}}{\alpha_2}\xi} \tag{2.6}$$

while the general solution to Eq. (2.5) is given by:

$$T = -\frac{\dot{q}'''}{\rho C V_{ad}}\xi + B_1 + B_2 e^{\frac{V_{ad}}{\alpha_2}\xi} \tag{2.7}$$

where A_1, A_2, B_1, B_2 are arbitrary integration constants. The asymptotic boundary conditions are given by:

$$T(\xi \to \infty) = T_0$$
$$T(0) = T_{cs}$$
$$\frac{\partial T}{\partial \xi}(\xi \to \infty) = 0$$
$$\left\| \frac{\partial T}{\partial \xi}(\xi \to -\infty) \right\| < \infty$$
$$\frac{\partial T}{\partial \xi}(\xi \to 0^+) = \frac{\partial T}{\partial \xi}(\xi \to 0^-)$$

where the first two boundary conditions give the value of the temperature at two known points (in the non-perturbed state and at the front), the third and fourth conditions are used in order to avoid a diverging solution, and the last condition assures continuity in the first derivative of the temperature at the front location. These 5 conditions are used to eliminate the 4 arbitrary constants and to determine the additional parameter V_{ad}, given by

$$V_{ad} = \sqrt{\frac{\dot{q}'''|\alpha_2|}{\rho C(T_{cs} - T_0)}} \tag{2.8}.$$

Second order accurate algorithm (n=3).

The general solution of the homogeneous Eq. (2.4) is:

$$T = A_1 + A_2 e^{-\sqrt{\frac{V_{ad}}{\alpha_3}}\xi} + A_3 e^{-\sqrt{\frac{V_{ad}}{\alpha_3}}\xi} \tag{2.9}$$

while the general solution to Eq. (2.5) is obtained similarly as:

$$T = -\frac{\dot{q}'''}{\rho C V_{ad}}\xi + B_1 + B_2 e^{-\sqrt{\frac{V_{ad}}{\alpha_3}}\xi} + B_3 e^{-\sqrt{\frac{V_{ad}}{\alpha_3}}\xi} \tag{2.10}$$

where A_1, A_2, A_3, B_1, B_2, B_3 are again arbitrary integration constants. The set of boundary conditions for this case are:

$$T\left(\xi \to \infty\right) = T_0$$

$$T\left(0\right) = T_{cs}$$

$$\frac{\partial T}{\partial \xi}\left(\xi \to \infty\right) = 0$$

$$\frac{\partial^2 T}{\partial \xi^2}\left(\xi \to \infty\right) = 0$$

$$\left\| \frac{\partial T}{\partial \xi}\left(\xi \to -\infty\right) \right\| < \infty$$

$$\frac{\partial T}{\partial \xi}\left(\xi \to 0^+\right) = \frac{\partial T}{\partial \xi}\left(\xi \to 0^-\right)$$

$$\frac{\partial^2 T}{\partial \xi^2}\left(\xi \to 0^+\right) = \frac{\partial^2 T}{\partial \xi^2}\left(\xi \to 0^-\right)$$

where with respect to the previous case, additional regularity conditions have been added on the second derivative terms in the temperature distribution. The resulting expression for the additional front speed V_{ad} is given by

$$V_{ad} = \left(\left(\frac{\dot{q}'''}{2\rho C\left(T_{cs} - T_0\right)} \right)^2 \alpha_3 \right)^{1/3} \qquad (2.11).$$

Appendix 3 List of Symbols

α	diffusivity
A_c	conductor cross section
A_h	fluid (helium) cross section
C	specific heat
$\hat{C}_v$	average fluid (helium) specific heat at constant volume
$\hat{C}_t$	averaged specific heat of conductor and helium coolant
C_c	conductor specific heat
C_v	fluid (helium) constant volume specific heat
D_h	hydraulic diameter
Δt	time step
Δx	space step
ε	relative error on the front position
f	friction factor
ϕ	Gruneisen parameter of fluid (helium)
$H(\xi)$	Heavyside function
k	thermal conductivity
p	fluid (helium) pressure
p_0	initial pressure
$\dot{q}'''$	heating rate per unit volume
ρ	fluid (helium) density
R	gas constant
ρ_c	conductor density
T	temperature
t	time
T_{cs}	current sharing temperature (transition superconducting > normal conducting)
v	fluid (helium) velocity
v^{num}	approximated fluid flow velocity as computed numerically
V_{ad}	additional propagation velocity of the normal front (due to numerical errors)
V_q	velocity of the normal front
V_q^{an}	velocity of the normal front as computed analytically
V_q^{num}	velocity of the normal front as computed numerically
ξ	moving coordinate
x	space coordinate
X_q	position of the normal front
X_q^{an}	position of the normal front as computed analytically
X_q^{num}	position of the normal front as computed numerically
X_{q0}	initial position of the normal front